Received 26 February 2019; accepted 5 March 2019. Date of publication 26 February 2019; date of current version 26 March 2019.

The review of this paper was arranged by Editor C. C. McAndrew.

Digital Object Identifier 10.1109/JEDS.2019.2903854

Compact Charge Modeling of Double-Gate MOSFETs Considering the Density-Gradient Equation

SUNG-MIN HONG[®] (Member, IEEE)

School of Electrical Engineering and Computer Science, Gwangju Institute of Science and Technology, Gwangju 61663, South Korea

CORRESPONDING AUTHOR: S.-M. HONG (e-mail: smhong@gist.ac.kr)

This work was supported by the Basic Science Research Program through the National Research Foundation of Korea (NRF) funded by the Ministry of Education under Grant NRF-2018R1D1A1B07048277.

ABSTRACT A compact charge model for double-gate metal-oxide-semiconductor field-effect transistors with the quantum confinement effect is presented. In addition to the Poisson equation, the density-gradient equation with a realistic boundary condition is considered to include the quantum confinement effect. The coupled governing equations are rigorously integrated. Contribution of the density-gradient equation is clearly identified. Based on the resultant integrated equation, a compact charge model is proposed. Expressions for model parameters are found. Numerical examples for various double-gate MOS structures are shown.

INDEX TERMS Compact model, density-gradient equation, double-gate MOSFETs, quantum confinement effect, semiconductor device modeling.

I. INTRODUCTION

Multigate Metal-Oxide-Semiconductor Field-Effect Transistors (MOSFETs) such as FinFETs [1]–[3] and nanowire FETs [4], [5] have become the major transistor technologies. The FinFETs are currently in the mass production. It is expected that the gate-all-around (GAA) transistors with superior gate controllability will be introduced soon. For example, recently, development of a nanosheet transistor has been reported [6]. Therefore, it is mandatory for the compact models to take into account multigate MOSFETs appropriately.

A fundamental step in building a compact model is to establish the charge-voltage characteristics of the given MOS structure. In order to model the charge-voltage characteristics in the multigate MOSFET accurately, two important factors – the shape of the cross-section and the quantum confinement effect – should be properly considered.

In the case of the geometric effect, recent compact models for multigate MOSFETs [7]–[11] are based on the "equivalent double-gate MOSFET model" concept. In those works, a general charge-voltage relation is defined and only

parameter values are dependent on the cross-section. It has been recently shown that an equivalent double-gate MOSFET model can be derived for an arbitrary cross-section by neglecting the non-uniformity of the surface potential [12].

In the case of the quantum confinement effect, there are various approaches. For example, the distance between the electron centroid and the semiconductor-insulator interface, which depends on the gate voltage, is added to the oxide thickness [11]. In [10], a quantum correction term is added to the core equation with an adjustable parameter. In another approach [13], [14], analytic solutions of the Schrödinger equation are used to calculate the inversion carrier density. Although the expression for the electron density is physically sound, coupling the electron density and the surface potential requires additional approximations [15].

As much as the device simulation is concerned, the density-gradient equation [16] is a *de facto* standard method to consider the quantum confinement effect. Therefore, a compact model, which considers the density-gradient equation together with the Poisson equation, is expected to significantly increase the transferability of the device

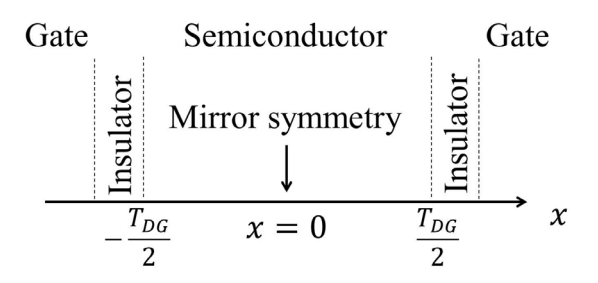


FIGURE 1. Double-gate structure whose thickness is T_{DG} . The center of the substrate is located at x = 0.

simulation into the compact model. To the best of the author's knowledge, it is difficult to find previous works on the compact model with the density-gradient equation.

In this work, a compact charge model for double-gate MOSFETs, where the quantum confinement is naturally included, is proposed. The organization of the paper is as follows: In Section II, the geometry assumed in this work and the governing equations are introduced. In Section III, the coupled governing equations are rigorously integrated. In Section IV, a compact charge model is derived. In Section V, the numerical results for double-gate MOS structures are shown to demonstrate the validity of the proposed approach. Finally the conclusion is made in Section VI.

II. PROBLEM SPECIFICATION

A double-gate structure shown in Fig. 1 is considered. The thickness of the substrate is T_{DG} and the position x varies from $-\frac{1}{2}T_{DG}$ to $\frac{1}{2}T_{DG}$. Due to the symmetric operation, physical quantities have the mirror symmetry with respect to the center, x = 0. Therefore, the slope of any variable at x = 0 vanishes. In the following, only a half structure with x > 0 is explicitly considered.

Two governing equations and their boundary conditions are discussed. In the substrate region, the Poisson equation is given by

$$\frac{d^2\phi}{dr^2} + \frac{\rho}{\epsilon} = 0,\tag{1}$$

where ϕ is the electrostatic potential and ϵ is the permittivity of the semiconductor. Assuming the fully-depleted substrate, the net charge density, ρ , is

$$\rho = -qn + qN^{+} = -qS^{2} + qN^{+}, \tag{2}$$

where q is the absolute elementary charge, n is the electron density, S is the square root of the electron density, and N^+ is the net ionized doping density. For a p-type substrate, N^+ is negative. The boundary condition at the semiconductor-insulator interface, $x = \frac{1}{2}T_{DG}$, is given as

$$\epsilon \frac{d\phi}{dx}\Big|_{x=\frac{1}{2}T_{DG}} = C_{ins}(V_G - \Phi_{MS} - \phi), \tag{3}$$

where V_G is the gate voltage, Φ_{MS} is the workfunction difference between the metal and the intrinsic reference semiconductor, and C_{ins} is the insulator capacitance *per area*.

The second governing equation is the density-gradient equation [16], [17], which takes into account the quantum confinement effect. The equation and its boundary condition are repeated here to improve the readability. The density-gradient equation is given by

$$\frac{d^2S}{dx^2} + \frac{1}{2b_n} \left(\phi - V_T \log \frac{S^2}{n_{int}} \right) S = \frac{d^2S}{dx^2} - \frac{1}{2b_n} \phi_q S = 0, \quad (4)$$

where V_T is the thermal voltage, n_{int} is the intrinsic carrier density, and $\phi_q = -\phi + V_T \log \frac{S^2}{n_{int}}$ is the quantum correction. With the quantum correction, the electron density can be written as

$$n = n_{int} \exp\left(\frac{\phi + \phi_q}{V_T}\right). \tag{5}$$

The coefficient b_n for the semiconductor region is given by

$$b_n = \frac{\gamma \hbar^2}{12gm_n},\tag{6}$$

where m_n is the electron effective mass and \hbar is the reduced Planck constant. γ is a material-dependent coefficient. For example, in the case of silicon, $\gamma = 3.6$ is used in [17]. The boundary condition for the density-gradient equation may have various forms. The simplest one sets vanishingly small electron density at the interface. However, in this work, a penetrating boundary condition of S [18] is considered. The slope of S at the semiconductor-insulator interface is given as

$$\frac{dS}{dx}\Big|_{x=\frac{1}{2}T_{DG}} = -\frac{b_{n,ins}}{b_n x_p} S = -\frac{S}{l},\tag{7}$$

where $b_{n,ins}$ is for the insulator region and x_p is the penetration depth inside the insulator region. Therefore, the effective decaying length, l, can be easily calculated from b_n , $b_{n,ins}$, and the energy barrier height at the interface. In the case of the silicon-oxide interface, l is assumed to be 0.1 nm.

The two governing equations, (1) and (4), should be solved together. A self-consistent solution of two equations should be found to get the charge density on the cross-section. Of course, the numerical simulation using the discretization easily provides the solution. However, instead of solving two coupled equations numerically, our goal is to establish the seamless connection between the device simulation and the compact model. In the subsequent sections, a general modeling approach is presented in some detail.

III. INTEGRATION OF GOVERNING EQUATIONS

The central quantity of interest is the integrated charge density, which can be expressed as (with help of the Poisson equation, (1)),

$$Q_{t} = \int_{0}^{\frac{1}{2}T_{DG}} \rho dx = -\epsilon \int_{0}^{\frac{1}{2}T_{DG}} \frac{d^{2}\phi}{dx^{2}} dx.$$
 (8)

By applying the boundary condition, (3), and the mirror symmetry, it is readily found that

$$Q_t = -\epsilon \frac{d\phi}{dx}\Big|_{x=\frac{1}{2}T_{DG}} = -C_{ins}(V_G - \Phi_{MS}) + C_{ins}\phi_s, \quad (9)$$

where $\phi_s = \phi(\frac{1}{2}T_{DG})$ is the surface potential. In a similar way, the subscript s is used to denote the quantity evaluated at $x = \frac{1}{2}T_{DG}$. In addition to Q_t , Q_e and Q_d are obtained by integrating the electron charge and the net doping charge,

$$Q_{e} = \int_{0}^{\frac{1}{2}T_{DG}} \left(-qS^{2}\right) dx = -\epsilon \frac{d\phi_{e}}{dx} \Big|_{x = \frac{1}{2}T_{DG}}$$
(10)

and

$$Q_d = \int_0^{\frac{1}{2}T_{DG}} (qN^+) dx = \frac{1}{2}T_{DG}qN^+ = -\epsilon \frac{d\phi_d}{dx} \Big|_{x = \frac{1}{2}T_{DG}}, \quad (11)$$

respectively. It is noted that Q_t , Q_e , and Q_d are the areal charge densities for the *half* structure.

In order to evaluate Q_t as a function of V_G , another equation is required to eliminate $C_{ins}\phi_s$. When the density-gradient equation is neglected for the double-gate MOSFET, the task can be achieved by integrating the Poisson equation along the position [19]. However, when the density-gradient equation is employed, two governing equations should be considered simultaneously. In this work, the density-gradient equation is integrated with a weighting factor, $\frac{dS}{dt}$.

Each term of the density-gradient equation, (4), is multiplied by the weighting factor, $\frac{dS}{dx}$. The first term of (4) is easily converted into

$$\frac{dS}{dx}\frac{d^2S}{dx^2} = \frac{1}{2}\frac{d}{dx}\left[\left(\frac{dS}{dx}\right)^2\right].$$
 (12)

By recalling $n = S^2$, the second term of (4) reads

$$\frac{dS}{dx}\frac{\phi S}{2b_n} = \frac{\phi}{4b_n}\frac{dn}{dx} = \frac{d}{dx}\left(\frac{\phi n}{4b_n}\right) - \frac{d\phi}{dx}\frac{n}{4b_n}.$$
 (13)

A term of $\frac{d\phi}{dx}n$ requires further manipulation. By using the Poisson equation, (1), it is identified

$$\frac{d\phi}{dx}n = \frac{d\phi}{dx} \left(\frac{\epsilon}{q} \frac{d^2\phi}{dx^2} + N^+ \right)
= \frac{\epsilon}{2q} \frac{d}{dx} \left[\left(\frac{d\phi}{dx} \right)^2 \right] + \frac{d}{dx} (\phi N^+).$$
(14)

The third term of the density-gradient equation is written as

$$-\frac{dS}{dx}\frac{V_TS}{2b_n}\log\frac{S^2}{n_{int}} = -\frac{V_T}{4b_n}\frac{dn}{dx}\log\frac{n}{n_{int}}$$
$$= \frac{d}{dx}\left[\frac{V_Tn}{4b_n}\left(1 - \log\frac{n}{n_{int}}\right)\right]. \quad (15)$$

Using (13), (14), (15), and the definition of ϕ_q , the density-gradient equation multiplied by $\frac{dS}{dx}$ can be written as

$$\frac{1}{2} \frac{d}{dx} \left[\left(\frac{dS}{dx} \right)^2 \right] - \frac{\epsilon}{8qb_n} \frac{d}{dx} \left[\left(\frac{d\phi}{dx} \right)^2 \right]
- \frac{d}{dx} \left(\frac{\phi N^+}{4b_n} \right) + \frac{d}{dx} \left[\frac{V_T n}{4b_n} \left(1 - \frac{\phi_q}{V_T} \right) \right] = 0.$$
(16)

When the above equation is integrated from 0 to $\frac{1}{2}T_{DG}$, all terms can be readily evaluated as

$$-\frac{2qb_n}{\epsilon} \left(\frac{dS}{dx}\right)^2 \Big|_{x=\frac{1}{2}T_{DG}} + \frac{1}{2} \left(\frac{d\phi}{dx}\right)^2 \Big|_{x=\frac{1}{2}T_{DG}} + (\phi_s - \phi_0) \frac{qN^+}{\epsilon} - n_s \left(1 - \frac{\phi_{qs}}{V_T}\right) \frac{qV_T}{\epsilon} + n_0 \left(1 - \frac{\phi_{q0}}{V_T}\right) \frac{qV_T}{\epsilon} = 0,$$

$$(17)$$

where a common coefficient of $-\frac{\epsilon}{4qb_n}$ is factored out for clarity and all quantities with a subscript 0 (such as n_0 , ϕ_0 , and ϕ_{q0}) are quantities evaluated at x=0. By applying the boundary condition, (7), we have

$$\frac{1}{2} \left(\frac{d\phi}{dx} \right)^{2} \Big|_{x = \frac{1}{2}T_{DG}} + (\phi_{s} - \phi_{0}) \frac{qN^{+}}{\epsilon} \\
- n_{s} \left(1 + \frac{2b_{n}}{l^{2}V_{T}} - \frac{\phi_{qs}}{V_{T}} \right) \frac{qV_{T}}{\epsilon} + n_{0} \left(1 - \frac{\phi_{q0}}{V_{T}} \right) \frac{qV_{T}}{\epsilon} = 0. \quad (18)$$

Three remarks would be instructive. Firstly, it is noted that no additional approximation has been introduced in the derivation procedure of (18). Although it is written in a different way, it is still a general relation. Secondly, it is stressed that (18) is an integrated equation. Although it is a general relation, it is another task to calculate the terms in (18). For example, the potential difference between the interface and the center, $\phi_s - \phi_0$, is difficult to calculate from (18) itself. In principle, it is required to integrate the Poisson equation twice to get the potential difference. However, when the density-gradient equation is included, an analytic solution for the overall system cannot be obtained easily. Modeling of such quantities are required and it will be done in Sections IV and V.

Finally, when the density-gradient equation is not considered, the semi-classical Poisson equation, where $S^2 = n = n_{int} \exp\left(\frac{\phi}{V_T}\right)$ is instead used, should be integrated. Following a similar procedure, the semi-classical version of (18) can be found as,

$$\frac{1}{2} \left(\frac{d\phi}{dx} \right)^2 \Big|_{x = \frac{1}{2} T_{DG}} + (\phi_s - \phi_0) \frac{qN^+}{\epsilon} - (n_s - n_0) \frac{qV_T}{\epsilon} = 0.$$
 (19)

By comparing (18) and (19), it is clearly seen that the density-gradient equation introduces additional terms. The last two terms of the left-hand side in (18) are related with the quantum correction. Therefore, the approach in this work enables a smooth transition between the semi-classical model to the quantum-corrected model.

IV. COMPACT CHARGE MODEL

Based on the integrated equation, (18), a compact charge model is established. For that purpose, all terms should be expressed as functions of the integrated charge densities. From (9), the first term of (18) can be easily identified as $\frac{1}{2\sqrt{2}}Q_t^2$.

 $\begin{array}{l} \frac{1}{2\epsilon^2}Q_t^2. \\ \text{The second term contains } \phi_s-\phi_0. \text{ Since } \phi_s-\phi_0 \text{ should} \\ \text{be expressed as a function of the integrated charge densities} \end{array}$

VOLUME 7, 2019 411

 $(Q_e \text{ and } Q_d)$, it is convenient to decompose the electrostatic potential into two terms, ϕ_e and ϕ_d ,

$$\phi = \phi_e + \phi_d, \tag{20}$$

which are defined as

$$\frac{d^2\phi_e}{dx^2} - \frac{qS^2}{\epsilon} = 0, (21)$$

$$\frac{d^2\phi_d}{dx^2} + \frac{qN^+}{\epsilon} = 0, (22)$$

respectively. From the source term of (21), it is easily recognized that ϕ_e is the electrostatic potential due to the electrons. On the other hand, ϕ_d is related with the dopants. As much as the boundary conditions of (21) and (22) are concerned, the following conditions are imposed. When the gate voltage is much smaller than the threshold voltage, the contribution of the electron becomes negligible. In other words, the electrostatic potential approaches to ϕ_d . Therefore, the boundary condition, (3), is also decomposed as

$$\epsilon \frac{d\phi_e}{dx}\Big|_{x=\frac{1}{2}T_{DG}} = -C_{ins}\phi_e, \tag{23}$$

$$\epsilon \frac{d\phi_d}{dx}\Big|_{x=\frac{1}{2}T_{DG}} = C_{ins}(V_G - \Phi_{MS} - \phi_d). \tag{24}$$

With these boundary conditions, ϕ_d is the electrostatic potential obtained by neglecting the electrons, while ϕ_e considers the correction only due to the electrons.

In order to calculate the potential difference, $\phi_s - \phi_0$, not only the integrated charges but also the charge centroids are required. From (22) and (11), it is found that the uniformly distributed doping density yields the following relation for ϕ_d ,

$$\frac{1}{2} \frac{d\phi_d}{dx} \Big|_{x = \frac{1}{2} T_{DG}} = -\frac{1}{2} \frac{Q_d}{\epsilon} = (\phi_{ds} - \phi_{d0}) \frac{2}{T_{DG}}, \quad (25)$$

where the factor of $\frac{1}{2}$ comes from the uniform distribution. In the case of ϕ_e , we cannot expect the same relation, because the electron density is not uniformly distributed. Depending on the relative position of the electron centroid, the factor can vary. When the electron centroid is close to the semiconductor-insulator interface, under the given surface field, the potential difference, $\phi_{es} - \phi_{e0}$, becomes smaller. Let us define the normalized distance between the electron centroid and the interface, α , as

$$1 - \alpha = \frac{2}{T_{DG}} \frac{\int_0^{\frac{1}{2}T_{DG}} xS^2 dx}{\int_0^{\frac{1}{2}T_{DG}} S^2 dx},$$
 (26)

where $\alpha = 0$ and 1 represent the electrons centered at the interface and the center, respectively. With the above definition of α and (21), it is found that

$$\alpha \frac{d\phi_e}{dx}\Big|_{x=\frac{1}{2}T_{DG}} = -\alpha \frac{Q_e}{\epsilon} = (\phi_{es} - \phi_{e0}) \frac{2}{T_{DG}}.$$
 (27)

Then, after a simple manipulation, we have

$$\begin{split} &\frac{1}{\epsilon^2}Q_e\bigg[\frac{1}{2}Q_e + (1-\alpha)Q_d\bigg]\\ &-n_s\bigg(1 + \frac{2b_n}{l^2V_T} - \frac{\phi_{qs}}{V_T}\bigg)\frac{qV_T}{\epsilon} + n_0\bigg(1 - \frac{\phi_{q0}}{V_T}\bigg)\frac{qV_T}{\epsilon} = 0. \end{split} \tag{28}$$

Following the approach in [9], an expression for ϕ_s is found as

$$\frac{qV_T}{\epsilon}n_{int}\exp\left(\frac{\phi_s}{V_T}\right) = \frac{\frac{1}{\epsilon^2}Q_e\left[\frac{1}{2}Q_e + (1-\alpha)Q_d\right]}{\eta_s - \exp\left(-\frac{\phi_s - \phi_0}{V_T}\right)\eta_0},\quad(29)$$

where two dimensionless coefficients (η_0 and η_s) are defined as

$$\eta_0 = \left(1 - \frac{\phi_{q0}}{V_T}\right) \exp\left(\frac{\phi_{q0}}{V_T}\right),\tag{30}$$

$$\eta_s = \left(1 + \frac{2b_n}{l^2 V_T} - \frac{\phi_{qs}}{V_T}\right) \exp\left(\frac{\phi_{qs}}{V_T}\right),\tag{31}$$

respectively. Since the potential difference can be expressed in terms of the integrated charge densities, we have

$$\phi_s = V_T \log \frac{Q_e \left[\frac{1}{2} Q_e + (1 - \alpha) Q_d \right]}{q \epsilon V_T n_{int} \left[\eta_s - \exp \left(\frac{\alpha Q_e + \frac{1}{2} Q_d}{\epsilon V_T} \frac{T_{DG}}{2} \right) \eta_0 \right]}.$$
 (32)

For the verification purpose, the numerical solution of the density-gradient equation is required. The silicon doublegate MOSFETs are numerically simulated in our in-house device simulation program, G-Device [20], [21]. The densitygradient equation, (4), and its boundary condition, (7), are newly implemented in the in-house simulator. In Fig. 2, the simulation results of the in-house simulator have been compared with those of the commercial device simulator, Sentaurus Device [22]. A thin and lightly-doped substrate $(T_{DG} = 4 \text{ nm and } (|N^+| = 10^{16} \text{ cm}^{-3}) \text{ and a thick}$ and heavily-doped substrate ($T_{DG} = 10$ nm and $|N^{+}| =$ 10^{19} cm^{-3}) are considered. The effective oxide thickness of the insulator layer is 0.5 nm throughout this work. The gate workfunction is assumed to be 4.3 eV. The quantum confinement effect is included and l is 0.1 nm. γ is assumed to be 3.6 [17]. Excellent agreement is achieved. The classical solutions of the same devices are also shown ("No QM" in the figure). The impact of the quantum confinement effect is clearly demonstrated.

Since the above equation, (32), is the central achievement in this work, its numerical verification is made. The surface potential obtained from the numerical simulation is shown as a function of the electron sheet density, $N_e = -\frac{Q_e}{q}$, in Fig. 3. The right-hand side term of (32) is also calculated by using the quantities, α , η_0 , and η_s , which are extracted from the numerical simulation results. It matches to the surface potential perfectly because (32) is an exact relation. For comparison, the result without the quantum confinement effect is shown for the thin and lightly-doped ($T_{DG} = 4$ nm and $|N^+| = 10^{16}$ cm⁻³) structure. Again, the impact

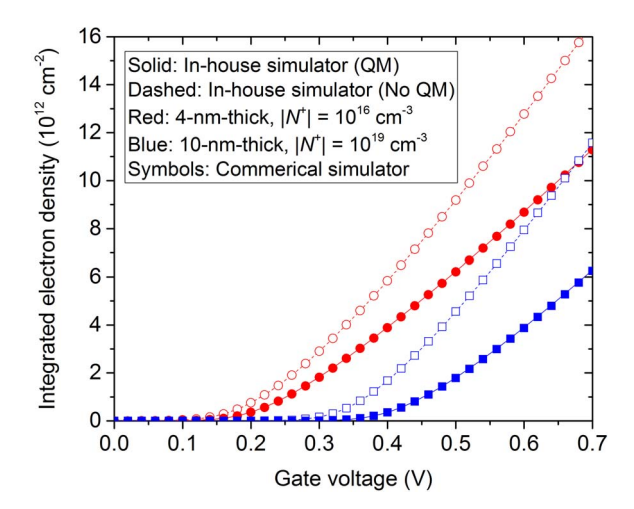


FIGURE 2. Integrated electron density as a function of the gate voltage. The silicon double-gate MOSFETs are numerically simulated by solving the density-gradient equation ("QM"). Excellent agreement is achieved between the simulation results obtained by the two device simulators (the in-house simulator and the commercial simulator). For comparison, the results without the quantum confinement effect ("No QM") are also shown.

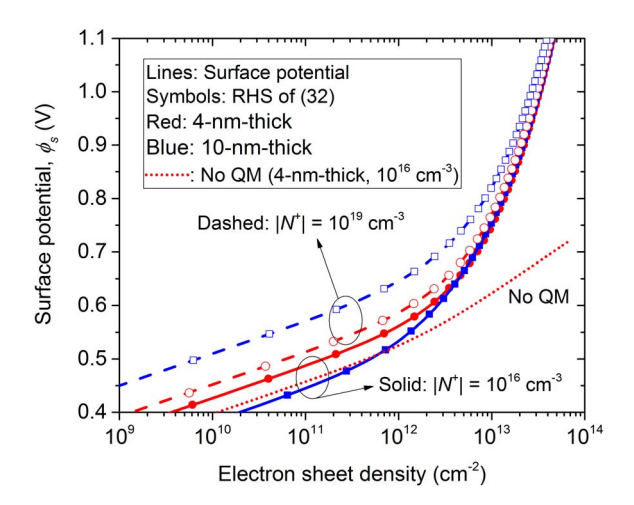


FIGURE 3. Surface potential, ϕ_s , and the right-hand side (RHS) term of (32) are shown as functions of the electron sheet density, $N_{\rm e}=-\frac{Q_{\rm e}}{q}$. Two different thicknesses (4 nm and 10 nm) and two p-type doping densities ($|N^+|=10^{16}$ and 10^{19} cm $^{-3}$) are considered. For comparison, the result without the quantum confinement effect is shown for the thin and lightly-doped ($T_{DG}=4$ nm and $|N^+|=10^{16}$ cm $^{-3}$) structure.

of the quantum confinement effect is clearly demonstrated. It is a remaining task to model parameters like α , η_0 , and η_s properly.

One interesting observation can be made in the semiclasscial case without the density-gradient equation, where both of η_0 and η_s become unity. In such a case, the expression for ϕ_s becomes very similar to the one in [9], except for different coefficients of the integrated charge densities. A heuristic fitting coefficient for Q_e^2 term was introduced in [9] and the resultant value was close to 0.5 regardless of the device structure. It is not accidental at all because the rigorous treatment in (32) reveals that the coefficient for Q_e^2 should be 0.5

Finally, by combining (9) and (32), the following equation is established,

$$V_G - \Phi_{MS} + \frac{Q_d}{C_{ins}} = \frac{-Q_e}{C_{ins}} + V_T \log \frac{Q_e \left[\frac{1}{2}Q_e + (1-\alpha)Q_d\right]}{q\epsilon V_T n_{int} \eta_{tot}}, (33)$$

where

$$\eta_{tot} = \eta_s - \exp\left(\frac{\alpha Q_e + \frac{1}{2}Q_d}{\epsilon V_T} \frac{T_{DG}}{2}\right) \eta_0$$
(34)

is introduced for notational simplicity.

V. PARAMETER MODELING FOR INTRINSIC DEVICES

Up to now, we have derived a compact charge model, (33), with the quantum confinement effect. For a given gate voltage, Q_e can be calculated by solving (33) as much as α and η_{tot} are fixed or expressed as functions of Q_e . Unfortunately, rigorous and compact equations for α and η_{tot} are not easily found. As an alternative approach, these parameters are modeled with empirical expressions in this work. In this section, the modeling procedures for α and η_{tot} are briefly presented.

When α and η_{tot} are modeled, they can be dependent on various simulation conditions like N_e , $|N^+|$, and T_{DG} . In this work, for the sake of simplicity, only intrinsic substrates $(|N^+|=0 \text{ and } Q_d=0)$ are considered. We will concentrate on their N_e -dependence at a certain T_{DG} value. Full investigation on the $|N^+|$ - and T_{DG} -dependence of α and η_{tot} will be reported elsewhere.

Firstly, α is investigated. As already discussed in Sections III and IV, α cannot be directly obtained from (18) itself. Proper modeling on α is required. In order to understand its behavior, α is extracted from the numerical simulation results from a simple relation,

$$\alpha = \frac{\epsilon}{q} (\phi_s - \phi_0) \frac{2}{T_{DG} N_e} + \frac{1}{2} \frac{Q_d}{q N_e}.$$
 (35)

where Q_d vanishes for an intrinsic substrate. The extracted α is shown as a function of N_e in Fig. 4. As discussed in [23], α at a low N_e is close to 0.7 for a thin substrate. When the substrate becomes thicker, α at a low N_e is decreased. With higher V_G values, electrons are moved toward the interface and α is decreased.

An empirical model for α is suggested to describe the extracted α closely. Since α is related to the electron centroid, its modeling can be done in a similar way with the previous works for the electron centroid [23]–[25]. As one possible way for its modeling, inspired by the result in [24], an approximate expression for α has been found as

$$\left[1 - (1 - \alpha)^2\right]^3 = \beta_0 \frac{N_0}{N_0 + (1 - \alpha)N_a},\tag{36}$$

VOLUME 7, 2019 413

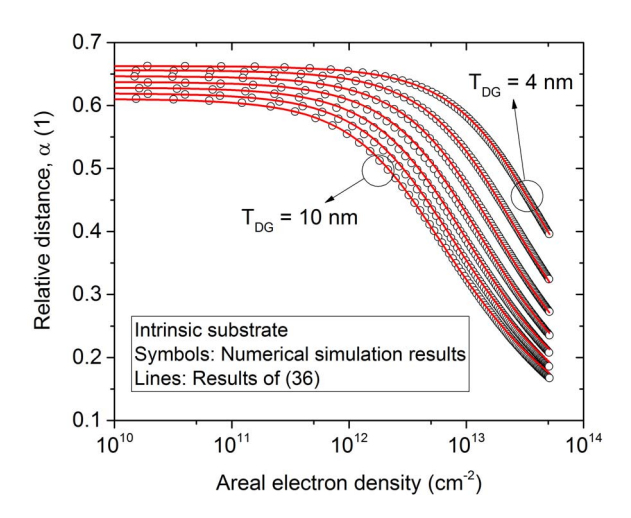


FIGURE 4. Extracted α as a function of $N_{\rm e}$ are shown as symbols. Lines represent results of the analytic expression in (36). Various T_{DG} values are considered and β_0 and N_0 are dependent on T_{DG} .

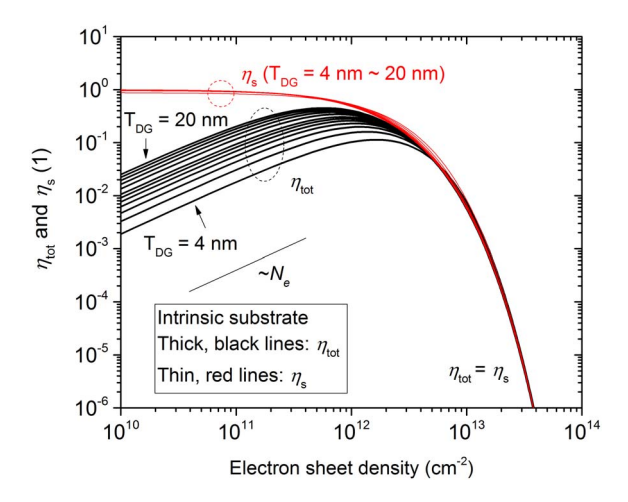


FIGURE 5. Extracted η_{tot} and η_s as functions of N_e . At high N_e values, η_{tot} is almost identical to η_s . At low N_e values, η_{tot} is a linear function of N_e .

where β_0 and N_0 are tuning parameters, which are dependent on T_{DG} . For example, when $T_{DG} = 5$ nm, the calibration yields $\beta_0 = 0.685$ and $N_0 = 1.02 \times 10^{13}$ cm⁻². With calibrated β_0 and N_0 , a good agreement can be obtained for various T_{DG} values, as shown in Fig. 4. It is stressed again that (36) is one of various possible relations to describe the extracted α as a function of N_e .

In addition to α , η_{tot} should be properly modeled. For various devices with intrinsic substrates (T_{DG} varying from 4 nm to 20 nm), η_{tot} and η_s are extracted from the numerical simulation results by using (34) and (31), respectively. The extracted η_{tot} and η_s are shown as functions of N_e in Fig. 5. At high N_e values, η_{tot} is solely determined by η_s because the contribution of $-\exp(\frac{\alpha Q_e}{\epsilon V_T}\frac{T_{DG}}{2})\eta_0$ becomes negligible. Furthermore, a linear dependence of η_{tot} on N_e is numerically confirmed at low N_e values.

Based upon the above observations, our approach to the modeling of η_{tot} is as follows: Two limiting cases for high

and low N_e values are separately modeled as η^L_{tot} and η^H_{tot} , respectively, and they are combined into an overall expression for η_{tot} . As much as η^H_{tot} is concerned, its modeling can be done by finding an expression for ϕ_{qs} . It is found that ϕ_{qs} is not much sensitive to T_{DG} . A fitting curve for ϕ_{qs} is found as

$$\phi_{qs}(N_e) = \phi_{qs}(0) \left[1 + \left(\frac{N_e}{N_1} \right)^{\beta_1} \right], \tag{37}$$

where $\phi_{qs}(0)$, β_1 , and N_1 are tuning parameters. In this specific example, $\phi_{qs}(0) = -0.13$ V, $\beta_1 = 0.77$ and $N_1 = 10^{13}$ cm⁻² are found. By using ϕ_{qs} obtained from the above expression and (31), η_{tot}^H can be readily available.

In the case of η_{tot}^L , a linear function with a T_{DG} -dependent proportional coefficient, β_2 , is tried as

$$\eta_{tot}^{L} = \beta_2 \frac{q}{\epsilon V_T} \frac{T_{DG}}{2} N_e. \tag{38}$$

Finally, two limiting expressions at high and low N_e values are merged into a single expression. It has been found that the following form is suitable for describing η_{tot} over the entire N_e range,

$$\frac{1}{\eta_{tot}(N_e)} \approx \frac{1}{\eta_{tot}^L(N_e)} + \frac{1}{\eta_{tot}^M} + \frac{1}{\eta_{tot}^H(N_e)},$$
 (39)

where η_{tot}^{M} is another tuning parameter to consider medium N_e values (around $10^{12}~{\rm cm}^{-2}$).

Since $\phi_{qs}(0)$, β_1 , and N_1 do not change much for various T_{DG} values, those parameters are treated as constants in this work. Therefore, tuning parameters, which are dependent on T_{DG} , are only β_2 and η^M_{tot} . This assumption greatly simplifies the tuning procedure. In Fig. 6, η_{tot} obtained from the numerical simulation and the results of (39) are compared. Values of $\phi_{qs}(0)$, β_1 , and N_1 are fixed. It is shown that η_{tot} can be accurately approximated by (39) with appropriately chosen β_2 and η^M_{tot} . When T_{DG} is 5 nm, a set of $\beta_2 = 0.219$ and $\eta^M_{tot} = 0.8$ is employed. For a 10-nm-thick device, $\beta_2 = 0.359$ and $\eta^M_{tot} = 4$.

In order to get the solution of (33), a set of equations (33), (36), and (39) – must be solved. Since α and η_{tot} depend on N_e nonlinearly, a self-consistent solution is calculated by using the Newton-Raphson method. One remark on the smoothness of the solution and its derivatives would be meaningful. Although α and η_{tot} depend on N_e nonlinearly, they are varying quite smoothly, as shown in Figs. 4 and 6. Moreover, each of α and η_{tot} is expressed with a single formula, which does not introduce any decomposition with respect to the operational regime. Therefore, as much as the numerical solution is obtained, its first and higher-order derivatives are smooth. It is also confirmed from our numerical experience.

In Fig. 7, the numerical results and the solutions of (33) are compared. Various T_{DG} values from 4 nm to 20 nm are considered. Excellent agreement is obtained as expected. The maximum peak error of the integrated electron density is less

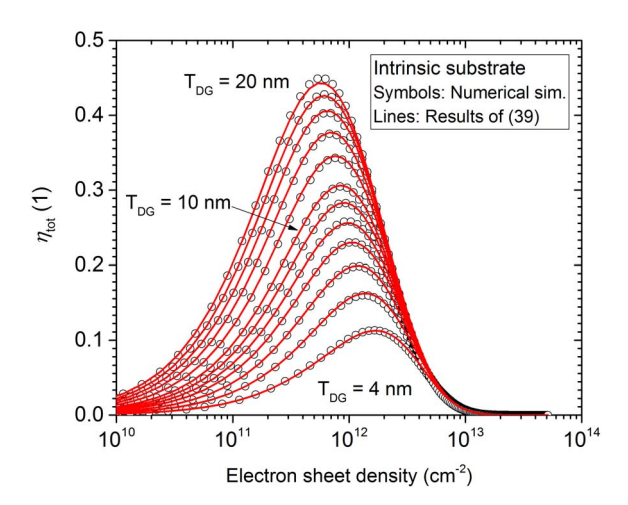


FIGURE 6. Comparison of η_{tot} (Lines) and its approximated expression, (39) (Symbols). Excellent agreement is obtained with $\phi_{qs}(0)=-0.13$ V, $\beta_1=0.77$ and $N_1=10^{13}$ cm $^{-2}$.

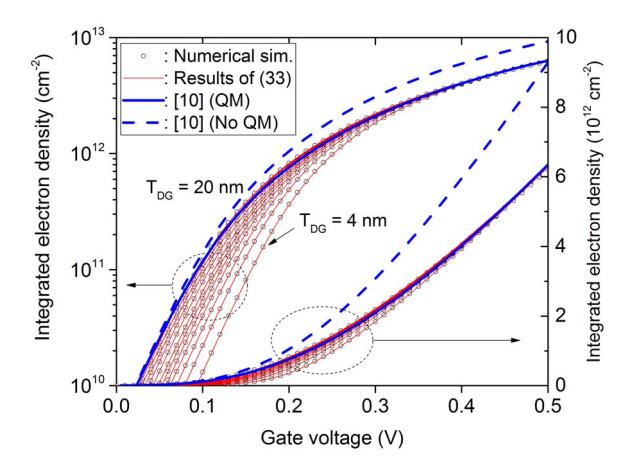


FIGURE 7. Integrated electron density as a function of the gate voltage. A magnified graph for gate voltages from 0 V to 0.5 V is drawn for clarity, although it has been tested up to 2 V with excellent agreement. Blue curves represent the results for the 20-nm-thick double-gate MOSFET, which are obtained by the model in [10].

than 2% for devices considered in this example. Such agreement is not accidental at all because (33) is an exact relation as much as α and η_{tot} are accurately modeled. It is noted that we have introduced some tuning parameters to describe η_{tot} . Although fitting those parameters is quite straightforward as much as the device simulation results are available, the tuning parameters generally deteriorate the predictability of the proposed model. Therefore, the dependence of α and η_{tot} on the simulation conditions (such as T_{DG} , $|N^+|$, and γ) would be an interesting topic for future research.

The comparison between our model and existing compact models would be of interest. Although the systematic benchmark test is beyond the scope of this work, the 20-nm-thick double-gate MOSFET is simulated by using the model presented in [10]. The model equation has been implemented into our simulation framework and the calculated results are shown as the blue curves in Fig. 7. In this particular

example, its dimensionless fitting parameter for the quantum confinement effect is adjusted to 0.3. Investigation on thinner structures is an interesting future research topic.

VI. CONCLUSION

In summary, a compact charge model of the double-gate MOSFET, (33), which is rigorously derived from the density-gradient equation and the Poisson equation, has been newly proposed. It has been clearly demonstrated that the quantum confinement effect introduces correction terms – η_0 and η_s – in the compact charge model. By modeling α and η_{tot} as functions of the integrated electron density, the charge-voltage characteristics of the intrinsic double-gate MOS structures have been accurately calculated. It is expected that the approach introduced in this work can be extended to various cross-sections of multigate MOSFETs. The calculation of the terminal currents is also a remaining step toward the full compact model for the double-gate MOSFET.

REFERENCES

- [1] C.-H. Jan et al., "A 22nm SoC platform technology featuring 3-D tri-gate and high-k/metal gate, optimized for ultra low power, high performance and high density SoC applications," in Proc. IEEE Int. Electron Devices Meeting (IEDM), Dec. 2012, pp. 3.1.1–3.1.4. doi: 10.1109/IEDM.2012.6478969.
- [2] S. Natarajan et al., "A 14nm logic technology featuring 2nd-generation FinFET, air-gapped interconnects, self-aligned double patterning and a 0.0588 μm² SRAM cell size," in Proc. IEEE Int. Electron Devices Meeting, Dec. 2014, pp. 3.7.1–3.7.3. doi: 10.1109/IEDM.2014.7046976.
- [3] S.-Y. Wu et al., "A 16nm FinFET CMOS technology for mobile SoC and computing applications," in Proc. IEEE Int. Electron Devices Meeting, Dec. 2013, pp. 9.1.1–9.1.4. doi: 10.1109/IEDM.2013.6724591.
- [4] R. Rurali, "Colloquium: Structural, electronic, and transport properties of silicon nanowires," *Rev. Mod. Phys.*, vol. 82, pp. 427–449, Feb. 2010. doi: 10.1103/RevModPhys.82.427.
- [5] S. Bangsaruntip *et al.*, "Density scaling with gate-all-around silicon nanowire MOSFETs for the 10 nm node and beyond," in *Proc. IEEE Int. Electron Devices Meeting*, Dec. 2013, pp. 20.2.1–20.2.4. doi: 10.1109/IEDM.2013.6724667.
- [6] N. Loubet *et al.*, "Stacked nanosheet gate-all-around transistor to enable scaling beyond finfet," in *Proc. VLSI Technol. Symp.*, 2017, pp. T230–T231. doi: 10.23919/VLSIT.2017.7998183.
- [7] J.-M. Sallese, N. Chevillon, F. Pregaldiny, C. Lallement, and B. Iniguez, "The equivalent-thickness concept for doped symmetric DG MOSFETs," *IEEE Trans. Electron Devices*, vol. 57, no. 11, pp. 2917–2924, Nov. 2010. doi: 10.1109/TED.2010.2071090.
- [8] N. Chevillon et al., "Generalization of the concept of equivalent thickness and capacitance to multigate MOSFETs modeling," *IEEE Trans. Electron Devices*, vol. 59, no. 1, pp. 60–71, Jan. 2012. doi: 10.1109/TED.2011.2171347.
- [9] J. P. Duarte et al., "A universal core model for multiple-gate field-effect transistors. Part I: Charge model," *IEEE Trans. Electron Devices*, vol. 60, no. 2, pp. 840–847, Feb. 2013. doi: 10.1109/TED.2012.2233478.
- [10] S. Khandelwal, J. P. Duarte, A. Medury, Y. S. Chauhan, and C. Hu, "New industry standard FinFET compact model for future technology nodes," in *Proc. VLSI Technol. Symp.*, Jun. 2015, pp. T62–T63. doi: 10.1109/VLSIT.2015.7223704.
- [11] O. Rozeau et al., "NSP: Physical compact model for stacked-planar and vertical gate-all-around MOSFETs," in Proc. IEEE Int. Electron Devices Meeting, Dec. 2016, pp. 7.5.1–7.5.4. doi: 10.1109/IEDM.2016.7838369.

VOLUME 7, 2019 415

- [12] S.-M. Hong and J. Park, "Substrate partitioning scheme for compact charge modeling of multigate MOSFETs," *IEEE J. Electron Devices Soc.*, vol. 5, no. 3, pp. 149–156, May 2017. doi: 10.1109/JEDS.2017.2682263.
- [13] G. Baccarani and S. Reggiani, "A compact double-gate MOSFET model comprising quantum-mechanical and nonstatic effects," *IEEE Trans. Electron Devices*, vol. 46, no. 8, pp. 1656–1666, Aug. 1999. doi: 10.1109/16.777154.
- [14] V. P. Trivedi and J. G. Fossum, "Quantum-mechanical effects on the threshold voltage of undoped double-gate MOSFETs," *IEEE Electron Device Lett.*, vol. 26, no. 8, pp. 579–582, Aug. 2005. doi: 10.1109/LED.2005.852741.
- [15] M. Shalchian, F. Jazaeri, and J.-M. Sallese, "Charge-based model for ultrathin junctionless DG FETs, including quantum confinement," *IEEE Trans. Electron Devices*, vol. 65, no. 9, pp. 4009–4014, Sep. 2018. doi: 10.1109/TED.2018.2854905.
- [16] M. G. Ancona and G. J. Iafrate, "Quantum correction to the equation of state of an electron gas in a semiconductor," *Phys. Rev. B, Condens. Matter.*, vol. 39, pp. 9536–9540, May 1989. doi: 10.1103/PhysRevB.39.9536.
- [17] A. Wettstein, A. Schenk, and W. Fichtner, "Quantum device-simulation with the density-gradient model on unstructured grids," *IEEE Trans. Electron Devices*, vol. 48, no. 2, pp. 279–284, Feb. 2001. doi: 10.1109/16.902727.
- [18] S. Jin, Y. J. Park, and H. S. Min, "A numerically efficient method for the hydrodynamic density-gradient model," in *Proc. Int. Conf. Simulat. Semicond. Process. Devices*, 2003, pp. 263–266. doi: 10.1109/SISPAD.2003.1233687.
- [19] Y. Taur, "An analytical solution to a double-gate MOSFET with undoped body," *IEEE Electron Device Lett.*, vol. 21, no. 5, pp. 245–247, May 2000. doi: 10.1109/55.841310.
- [20] S.-M. Hong and J.-H. Jang, "Numerical simulation of plasma oscillation in 2-D electron gas using a periodic steady-state solver," *IEEE Trans. Electron Devices*, vol. 62, no. 12, pp. 4192–4198, Dec. 2015. doi: 10.1109/TED.2015.2489220.

- [21] S.-M. Hong and J.-H. Jang, "Transient simulation of semiconductor devices using a deterministic Boltzmann equation solver," *IEEE J. Electron Devices Soc.*, vol. 6, pp. 156–163, 2018. doi: 10.1109/JEDS.2017.2780837.
- [22] Sentaurus Device User Guide, Synopsys Inc., Mountain View, CA, USA, 2014.
- [23] S. Venugopalan, M. A. Karim, S. Salahuddin, A. M. Niknejad, and C. C. Hu, "Phenomenological compact model for QM charge centroid in multigate FETs," *IEEE Trans. Electron Devices*, vol. 60, no. 4, pp. 1480–1484, Apr. 2013. doi: 10.1109/TED.2013.2245419.
- [24] J. He, M. Chan, X. Zhang, and Y. Wang, "An analytic model to account for quantum—mechanical effects of MOSFETs using a parabolic potential well approximation," *IEEE Trans. Electron Devices*, vol. 53, no. 9, pp. 2082–2090, Sep. 2006. doi: 10.1109/TED.2006.880359.
- [25] J. B. Roldan, A. Godoy, F. Gamiz, and M. Balaguer, "Modeling the centroid and the inversion charge in cylindrical surrounding gate MOSFETs, including quantum effects," *IEEE Trans. Electron Devices*, vol. 55, no. 1, pp. 411–416, Jan. 2008. doi: 10.1109/TED.2007.911096.



SUNG-MIN HONG (M'08) received the B.S. degree in electrical engineering and the Ph.D. degree in electrical engineering and computer science from Seoul National University, Seoul, South Korea, in 2001 and 2007, respectively.

He is currently an Assistant Professor with the School of Electrical Engineering and Computer Science, Gwangju Institute of Science and Technology, Gwangju, South Korea. His main research interest includes physics-based device modeling.